



Fluorinated derivatives of pyridine-2,4-dicarboxylate are potent inhibitors of human 2-oxoglutarate dependent oxygenases

Lennart Brewitz^a, Yu Nakashima^{a,b}, Anthony Tumber^a, Eidarus Salah^a, Christopher J. Schofield^{a,*}

^a Chemistry Research Laboratory, University of Oxford, 12 Mansfield Road, OX1 3TA, Oxford, United Kingdom

^b Present address: Institute of Natural Medicine, University of Toyama, 2630-Sugitani, 930-0194, Toyama, Japan

ARTICLE INFO

Keywords:

2-Oxoglutarate / α -ketoglutarate dependent oxygenase
 Pyridine-2,4-dicarboxylic acid / 2,4-PDCA
 JmjC lysine demethylase / KDM
 Aspartate/asparagine- β -hydroxylase / AspH / BAH / HAAH
 Ribosomal oxygenase 2 / RIOX2 / Mina53
 Fluorinated hydroxylase inhibitor

ABSTRACT

2-Oxoglutarate (2OG) oxygenases have important roles in human biology and are validated medicinal chemistry targets. Improving the selectivity profile of broad-spectrum 2OG oxygenase inhibitors may help enable the identification of selective inhibitors for use in functional assignment work. We report the synthesis of F- and CF₃-substituted derivatives of the broad-spectrum 2OG oxygenase inhibitor pyridine-2,4-dicarboxylate (2,4-PDCA). Their inhibition selectivity profile against selected functionally distinct human 2OG oxygenases was determined using mass spectrometry-based assays. F-substituted 2,4-PDCA derivatives efficiently inhibit the 2OG oxygenases aspartate/asparagine- β -hydroxylase (AspH) and the JmjC lysine-specific N^ε-demethylase 4E (KDM4E); The F- and CF₃-substituted 2,4-PDCA derivatives were all less efficient inhibitors of the tested 2OG oxygenases than 2,4-PDCA itself, except for the C5 F-substituted 2,4-PDCA derivative which inhibited AspH with a similar efficiency as 2,4-PDCA. Notably, the introduction of a F- or CF₃-substituent at the C5 position of 2,4-PDCA results in a substantial increase in selectivity for AspH over KDM4E compared to 2,4-PDCA. Crystallographic studies inform on the structural basis of our observations, which exemplifies how a small change on a 2OG analogue can make a substantial difference in the potency of 2OG oxygenase inhibition.

1. Introduction

2-Oxoglutarate (2OG)-dependent oxygenases couple two electron substrate oxidations with the oxidative decarboxylation of 2OG to give succinate and CO₂; they employ Fe(II) as a cofactor [1]. 2OG dependent hydroxylases have validated functions in human biology (Fig. 1a); for example, they act as sensors in the hypoxic response, *i.e.* the hypoxia inducible transcription factor-1 α (HIF-1 α) prolyl hydroxylases PHD1–3 together with the asparaginyl hydroxylase factor inhibiting the hypoxia inducible transcription factor-1 α (FIH) catalyze the hydroxylation of HIF- α substrates in an O₂-dependent manner [2]. Inhibiting human PHDs is of demonstrated therapeutic relevance for the treatment of anemia in patients with dialysis-dependent chronic kidney disease [3]. The development of potent and selective inhibitors for 2OG hydroxylases other than the PHDs is of basic scientific (for use in functional assignment studies) and therapeutic interest, in the latter case for diseases including cancer [4]. For example, aspartate/asparagine- β -hydroxylase (AspH), which catalyzes the stereoselective C3

hydroxylation of Asp/Asn-residues that are part of specific disulfide isomers of epidermal growth factor-like domains (EGFDs) [5–7], and certain JmjC lysine-specific N^ε-demethylases, which catalyze the N^ε-lysine demethylation of histones via initial N^ε-methyl-group hydroxylation followed by fragmentation to give formaldehyde as a coproduct (Supporting Figure S1), are current medicinal chemistry targets for cancer treatment [8–12].

Broad-spectrum 2OG oxygenase inhibitors are described, including the natural product N-oxalylglycine (NOG, 1; Fig. 1b) [13] and pyridine-2,4-dicarboxylate (2,4-PDCA, 2; Fig. 1c) [4]. These broad-spectrum inhibitors show distinct selectivity profiles; for example, 2,4-PDCA efficiently inhibits AspH and some JmjC KDMs [14, 15]. By contrast, 2,4-PDCA is only a weak inhibitor of the PHDs and of FIH [15], which catalyzes the stereoselective C3 hydroxylation of Asn/Asp/His/Ser/Leu-residues (Supporting Figure S1) [16, 17]. For other classes of human 2OG oxygenases, such as the ribosomal oxygenase 2 (RIOX2; MYC-induced nuclear antigen 53, MINA53), which catalyzes the stereoselective C3 hydroxylation of His39 of the 60S

* Corresponding author.

E-mail address: christopher.schofield@chem.ox.ac.uk (C.J. Schofield).

<https://doi.org/10.1016/j.jfluchem.2021.109804>

Received 15 March 2021; Received in revised form 30 April 2021; Accepted 1 May 2021

Available online 13 May 2021

0022-1139/© 2021 The Author(s). Published by Elsevier B.V. This is an open access article under the CC BY license (<http://creativecommons.org/licenses/by/4.0/>).

ribosomal protein L27a (RPL27A) [18], the potency of these broad-spectrum inhibitors has not been reported.

Introducing substituents on the scaffold of broad-spectrum 2OG oxygenase inhibitors is a viable strategy to enhance inhibitor selectivity. For example, substituting the glycine of NOG by D-phenylalanine led to the development of the (partially) selective FIH inhibitor *N*-oxalyl-D-phenylalanine (NOFD) [19]. Analogous strategies for the identification of more selective 2,4-PDCA-based 2OG oxygenase inhibitors by introducing substituents at the C3 position of the pyridine ring have been largely unsuccessful in improving the selectivity pattern of 2,4-PDCA [15, 20]. We anticipated that the introduction of F- and CF₃-substituents at the C3 and C5 position of the 2,4-PDCA scaffold might affect inhibitor selectivity due to the particular electronic and pharmacokinetic properties of fluorinated molecules, as being increasingly exploited in medicinal chemistry [21, 22]. Here we present proof-of-concept studies on how the introduction of substituents at the C5 position of 2,4-PDCA, which has not previously been investigated in structure activity relationship studies on 2OG oxygenases, increases the selectivity of 2,4-PDCA for AspH.

2. Results and discussion

2.1. Synthesis of F- and CF₃-substituted 2,4-PDCA derivatives

2,4-PDCA derivatives bearing F- or CF₃-substituents at the C3 or C5 position were synthesized from commercially sourced F- or CF₃-substituted isonicotinic acid derivatives in three or two steps, respectively, employing an analogous strategy to that used for the synthesis of C3 aminoalkyl-substituted 2,4-PDCA derivatives [15]. For example, 2-chloro-3-fluoroisonicotinic acid (**3**) was converted into its methyl ester, which was then submitted to Pd-catalyzed carbonylation [23] to afford dimethyl 3-fluoropyridine-2,4-dicarboxylate (**5**) (77%, over two steps; Scheme 1A). The purified 3-fluoropyridine-2,4-dicarboxylate (**7**), which is suitable for performing *in vitro* biochemical and biophysical studies as 2OG oxygenase inhibition, was obtained in 86% yield from dimethyl ester **5** after lithium hydroxide-mediated saponification and removal of excess base by acidic ion exchange chromatography. In a similar manner, 5-fluoropyridine-2,4-dicarboxylate (**8**) was obtained from 2-chloro-5-fluoroisonicotinic acid (**4**) (82%, over three steps; Scheme 1A). The corresponding purified 3- and 5-trifluoromethylated pyridine-2,4-dicarboxylates **13** and **14** were obtained in 79% and 89% yields, respectively, over two steps from the appropriate methyl trifluoromethylisonicotinic acid esters **9** and **10** (Scheme 1B).

2.2. F- and CF₃-substituted 2,4-PDCA derivatives inhibit human 2OG oxygenases

The ability of the synthetic F- or CF₃-substituted 2,4-PDCA derivatives **7**, **8**, **13**, and **14** to inhibit human 2OG oxygenases was assessed

with selected isolated recombinant enzymes (Table 1). 2,4-PDCA (**2**) was included in the assays to enable comparison of the effects of the F- or CF₃-substituents on the potency. Three representative human 2OG oxygenases, for which structures in complex with 2,4-PDCA have been reported, were employed in the inhibition studies: AspH [14], FIH [24], and KDM4E [25]. KDM4E was used as a representative JmjC KDM; it catalyzes the demethylation of histone 3 (H3) N^e-di- and trimethylated Lys9 (H3K9me3/me2) [10-12]. The inhibitory effect of 2,4-PDCA and its derivatives was also investigated for human RIOX2, though a structure of RIOX2 in complex with 2,4-PDCA has not yet been reported. A structure of the phylogenetically related ribosomal 2OG oxygenase RIOX1 (also known as nucleolar protein 66, NO66) with 2,4-PDCA (PDB ID: 4DIQ) suggests that 2,4-PDCA inhibits this subclass of 2OG oxygenases [26, 27]. Half maximum inhibitory concentrations (IC₅₀-values) of 2,4-PDCA and its four derivatives were determined using solid phase extraction coupled to mass spectrometry (SPE-MS) inhibition assays, which directly monitor peptide hydroxylation (+16 Da; for AspH [14, 28], FIH [29], RIOX2 [30]) or demethylation (-14 and -28 Da; for KDM4E [31]) (Supporting Figure S1).

The SPE-MS inhibition assays were of high quality as revealed by Z'-factors > 0.5 (Supporting Figure S2) [32]. The Hill slopes [33] of the inhibition curves of 2,4-PDCA and active derivatives were near the theoretical value of -1 (Supporting Figure S3), as predicted for single molecules competing with 2OG for binding to the active site. The IC₅₀-values of 2,4-PDCA (**2**) obtained for AspH, FIH, and KDM4E are in the ranges of those reported (Table 1) [15]. The inhibition of AspH by 2,4-PDCA is about an order of magnitude more efficient than of KDM4E as judged by IC₅₀-values (*i.e.* IC₅₀ ~ 0.03 μM for AspH and IC₅₀ ~ 0.29 μM for KDM4E; Table 1), in part reflecting the different assay conditions used (final assay concentrations: KDM4E: 0.15 μM; AspH: 0.05 μM; Table 1). As anticipated based on a crystal structure of RIOX1 in complex with 2,4-PDCA (PDB ID: 4DIQ), efficient inhibition of RIOX2 by 2,4-PDCA was observed (IC₅₀ ~ 4.0 μM, Table 1). 2,4-PDCA inhibits RIOX2 with similar potency as FIH (IC₅₀ ~ 4.7 μM, Table 1), *i.e.* more than two orders of magnitude less efficiently than it inhibits AspH. This information should be of use in the screening and design of improved RIOX2 inhibitors; RIOX2 is a proposed anti-cancer medicinal chemistry target [34].

The F- and CF₃-substituted 2,4-PDCA derivatives **7**, **8**, **13**, and **14** are all less efficient 2OG oxygenase inhibitors than 2,4-PDCA (Table 1), with the exception of the C5 F-substituted 2,4-PDCA derivative **8** which inhibits AspH with a similar potency as 2,4-PDCA (IC₅₀ ~ 0.05 and 0.03 μM, respectively). The reduced inhibition observed for the F- and CF₃-substituted 2,4-PDCA derivatives may reflect (in part) their weakened coordination to Fe(II) due to their reduced electron donating capacity caused by the electron withdrawing F- or CF₃-substituents. In general, the 2,4-PDCA derivatives bearing CF₃-substituents were less efficient 2OG oxygenase inhibitors than those bearing F-substituents (Table 1). Considering that the electron withdrawing effect of the F- and CF₃-

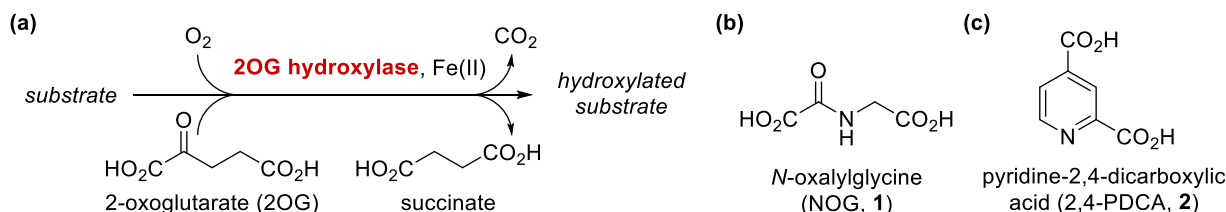
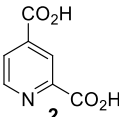
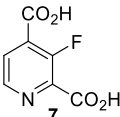
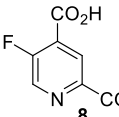
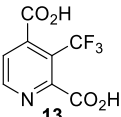
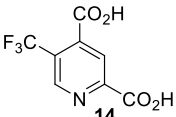


Fig. 1. 2OG hydroxylase catalysis and widely-used broad-spectrum inhibitors. a) 2OG hydroxylases couple substrate oxidation to the oxidative decarboxylation of 2OG using Fe(II) as a cofactor; b and c) the broad-spectrum 2OG oxygenase inhibitors: b) *N*-oxalylglycine (NOG, **1**) and c) pyridine-2,4-dicarboxylate (2,4-PDCA, **2**).

Table 1
F- and CF₃-substituted 2,4-PDCA derivatives inhibit human 2OG oxygenases.

					
	IC₅₀ [μM]	IC₅₀ [μM]	IC₅₀ [μM]	IC₅₀ [μM]	IC₅₀ [μM]
^{a,b} AspH	0.03 ± 0.01	0.11 ± 0.01	0.05 ± 0.01	>50	4.2 ± 1.0
^{a,c} FIH	4.7 ± 1.6	>50	>50	^d inactive	^d inactive
^{a,e} KDM4E	0.29 ± 0.05	1.3 ± 0.2	1.6 ± 0.3	^d inactive	^d inactive
^{a,d} RIOX2	4.0 ± 1.1	>50	>50	^d inactive	^d inactive

a) Mean of two independent runs (n = 2; mean ± SD); b) using 0.05 μM His₆-AspH_{315–758} and 1.0 μM of a thioether-linked cyclic peptide based on human coagulation factor X (hFX, amino acids 101–119; hFX-CP_{101–119}) [14, 28]; c) using 0.15 μM His₆-FIH and 5.0 μM HIF-1α C-terminal transactivation domain fragment (HIF-1α CAD, amino acids 788–822) [29]; d) 2,4-PDCA derivatives were termed inactive if 2OG oxygenase inhibition was not observed in the tested concentration range (100 – 0.002 μM) as shown in Supporting Figure S3; e) using 0.15 μM KDM4E and 10.0 μM of a variant of a histone 3 fragment (H3_{1–15}K9me3, amino acids 1–15) [31]; f) using 0.15 μM His₆-RIOX2_{26–465} and 5.0 μM of RPL27A_{31–49} peptide (Supplementary Information Section 5) [30].

substituents on the central pyridine heterocyclic ring are likely in the same range (the CF₃ group electronegativity is reported to be in the range of chlorine substituents [35]), the reduced 2OG oxygenase inhibition of 2,4-PDCA derivatives bearing CF₃-substituents might relate to the steric repulsion of the CF₃-substituent with side chains of active site residues; note, the A-value of a CF₃-group is between those of isopropyl- and *tert*-butyl-groups [36, 37]. Alternatively, it may relate to the interaction of the CF₃-substituent with the adjacent C4 (and C2 for 13) 2,4-PDCA derivative carboxylate groups, potentially limiting their ability to engage in interactions with the side chains of Arg735, His690, Arg688, and Ser668 and the active site metal ion due to limited rotational freedom. No activity of the C3 or C5 CF₃-substituted 2,4-PDCA derivatives 13 and 14 was observed against KDM4E, FIH, and RIOX2 (Table 1 and Supporting Figure S3), demonstrating how a relatively small modification to the broad-spectrum inhibitor 2,4-PDCA can cause a large difference in potency.

The IC₅₀-values for both the C3 and C5 F-substituted 2,4-PDCA derivatives increase in the order of AspH < KDM4E < FIH ~ RIOX2 (Table 1). Substantial inhibition was only observed for AspH and KDM4E, while incomplete inhibition curves or no inhibition was observed for FIH and RIOX2 (Supporting Figure S3). Notably, the inhibition of AspH by 2,4-PDCA derivatives bearing a CF₃- and, to a lesser extent, a F-substituent at the C5 position appears to be more efficient than by those bearing a CF₃- or F-substituent at the C3 position. Consequently, the C5 F-substituted 2,4-PDCA derivative 8 shows a threefold increase in selectivity for AspH over KDM4E with respect to 2,4-PDCA and the 2,4-PDCA derivative 7, and the C5 F-substituted 2,4-PDCA derivative 14 was only active against AspH, though much less potent than the C3 or C5 F-substituted 2,4-PDCA derivatives (Table 1).

2.3. Crystallography

To investigate the molecular reasons that determine why the inhibition of AspH by 2,4-PDCA derivatives bearing a CF₃- or F-substituent at the C5 position appears to be more efficient than by those bearing a CF₃- or F-substituent at the C3 position, crystallization studies with AspH and the fluorinated 2,4-PDCA derivatives were initiated. AspH was successfully crystallized in the presence of the F-substituted 2,4-PDCA derivatives 7 or 8, Mn(II) substituting for Fe(II), and the synthetic hFX-EGFD1_{86–124}-4Ser substrate peptide [6] (Supporting Figure S4), which mimics the EGFD1 of the reported AspH substrate human

coagulation factor X (hFX) [38, 39], whereas crystallization in the presence of the CF₃-substituted 2,4-PDCA derivatives 13 and 14 was unsuccessful. The structures were solved by molecular replacement using a reported AspH structure (PDB ID: 5JTC) [14] as a search model. In the presence of 7, AspH crystallized in the P2₁2₁2₁ space group (1.66 Å resolution, a single AspH molecule is in the asymmetric unit; Supporting Figure S5), in agreement with reported AspH structures [6, 14, 40]. By contrast, in the presence of 8, AspH crystallized in the P1 space group with two molecules in the asymmetric unit, both of which were observed to bind to the inhibitor, but only one of which was bound to the substrate (1.75 Å resolution; Supporting Figure S6).

Clear electron density for both 7 and 8 was observed in the AspH active site (Fig. 2a and b), in agreement with the 2OG competitive inhibition mechanism observed for 2,4-PDCA [14, 28]. Substituting 2,4-PDCA by the 2,4-PDCA derivative 7 or 8 in the AspH active site neither changes the overall protein fold nor the hFX-EGFD1_{86–124}-4Ser peptide conformation (Supporting Figures S7–S9). The F-substituted 2,4-PDCA derivatives bind to the AspH active site in a manner similar to 2,4-PDCA (Fig. 2c and d), i.e. the C2 carboxylates are positioned to interact with Arg688 (7: 2.8 Å; 8: 2.7 Å) and His690 (7: 2.9 Å; 8: 2.8 Å) and bind the metal ion (7: 2.2 Å; 8: 2.2 Å) together with the pyridine nitrogen atoms (7: 2.3 Å; 8: 2.3 Å); the C4 carboxylates are positioned to interact with Ser668 (7: 2.7 Å; 8: 2.6 Å) and Arg735 (7: 2.6 and 2.9 Å; 8: 2.6 and 3.1 Å).

The two AspH structures inform on the molecular rationale for the observed differences in the inhibitory potency of the C3 and C5 F-substituted 2,4-PDCA derivatives 7 and 8 and, by analogy, the C3 and C5 CF₃-substituted 2,4-PDCA derivatives 13 and 14 (Table 1). The F-substituent at the C3 position of 7 is in close proximity to the side chains of Ile737, Ile739, Ser668, and His690; bulkier substituents at the C3 position of 2,4-PDCA (such as the CF₃-group in 13) likely clash with these side chains hampering efficient binding of the molecules to the AspH active site (i.e. IC₅₀ > 50 μM for 13, Table 1). By contrast, the F-substituent at the C5 position of 8 faces towards the hydrophobic side chains of Val676 and Val727 which, together with those of Trp625 and Met670, form a more spacious hydrophobic pocket (compared to that available for C3 substituents), which can also accommodate bulkier substituents than F, e.g. the C5 CF₃-substituent of 14 (IC₅₀ ~ 4.2 μM, Table 1) [40]. The F-substituent of 8 can potentially engage in hydrophobic interactions with the proximal hydrophobic pocket of AspH, which could rationalize the observed similar potency of 8 and 2,4-PDCA

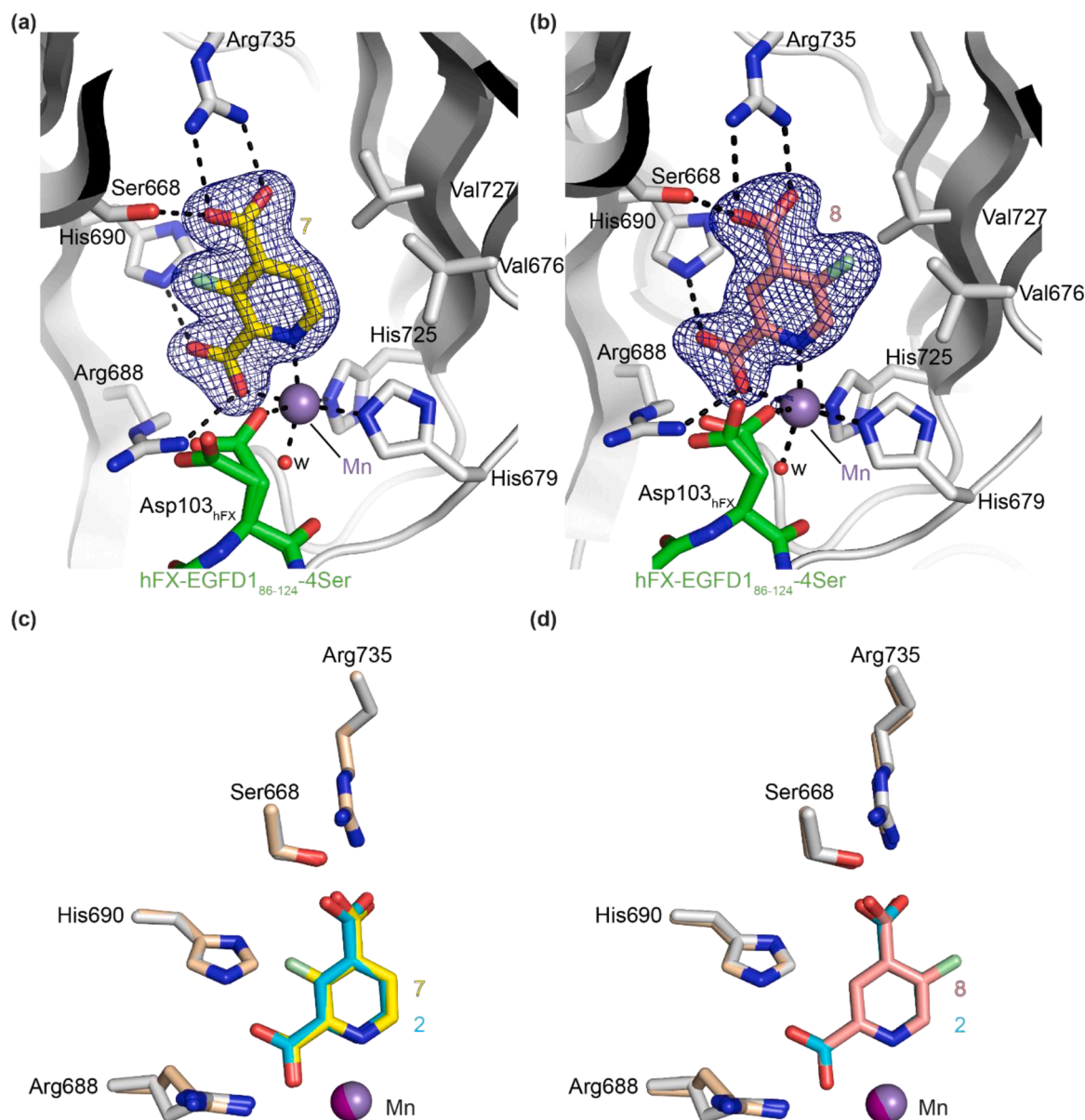


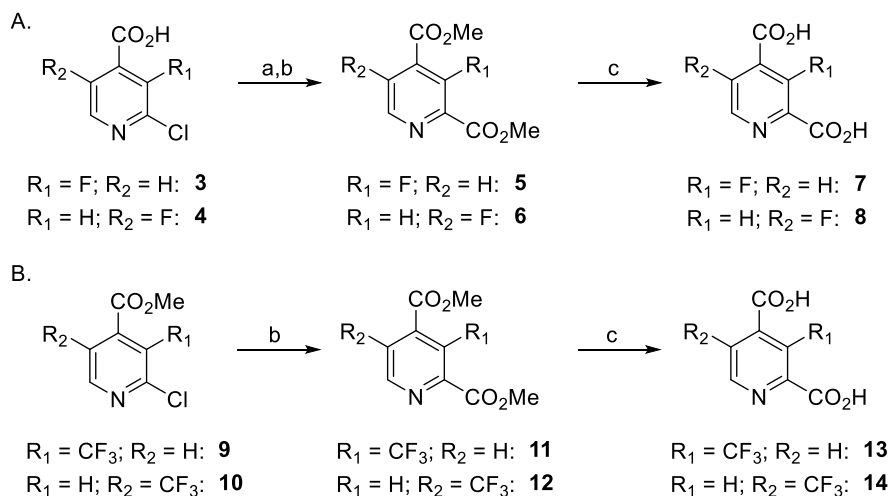
Fig. 2. Binding mode of C3 and C5 F-substituted 2,4-PDCA derivatives with AspH. Colors: gray: His₆-AspH₃₁₅₋₇₅₈; yellow: carbon-backbone of 3-fluoropyridine-2,4-dicarboxylate (**7**); salmon: carbon-backbone of 5-fluoropyridine-2,4-dicarboxylate (**8**); lavender blue: Mn; green: carbon-backbone of the hFX-EGFD1₈₆₋₁₂₄-4Ser peptide (Supporting Figure S4); red: oxygen; blue: nitrogen; pale green: fluorine. w: water. a and b) Representative OMIT electron density map (mF_o-DF_c) contoured to (a) 7.0σ around **7** of the AspH:**7** structure and (b) 7.0σ around **8** of the AspH:**8** structure, respectively; c and d) superimposition of a view of the AspH:**2** structure (pale brown: His₆-AspH₃₁₅₋₇₅₈; pink: Mn; cyan: carbon-backbone of 2,4-PDCA **2**) with (c) the AspH:**7** structure and (d) the AspH:**8** structure, respectively.

in inhibiting AspH ($IC_{50} \sim 0.05$ and $0.03 \mu\text{M}$, respectively).

We anticipate that the structure activity relationship results presented here will help to enable the development of 2OG competitive AspH inhibitors for use in validating AspH as a target for cancer therapy and diagnostics; AspH is reported to be upregulated on the surface of cancer cells potentially obviating the necessity for the 2,4-PDCA derivative to penetrate the cell wall [41, 42]. By contrast, most 2OG oxygenases are intracellular, including the RIOXs and JmjC KDMs, which are potential cancer targets [10-12, 30]. 2,4-PDCA dimylesters have been used in cell-based and *in vivo* inhibition studies of 2OG oxygenases [43, 44], the presence of hydrophobic F- or CF₃-substituents on the scaffold of 2,4-PDCA might further increase the cell-wall permeability of the 2,4-PDCA derivatives.

Other potential additional applications of the F-substituted 2,4-

PDCA derivatives include, for example, their use as electron deficient substrates for nucleophilic aromatic substitution reactions to label active site cysteine residues, which are present in the human DNA-modifying and 2OG-dependent ten-eleven translocation (TET) enzymes [45]. The F-substituted 2,4-PDCA derivatives may also be of use as ¹⁹F NMR probes in fluorine chemical shift anisotropy and exchange high-throughput screening for protein binding [46, 47]. Recent advances in fluorination reactions suitable for the rapid late-stage introduction of radioactive ¹⁸F atoms into heteroaromatic scaffolds [48, 49], including in substituted pyridines such as fluorinated derivatives of the multiple sclerosis drug 4-aminopyridine [50-52], suggest the F-substituted 2,4-PDCA derivatives might be useful scaffolds for positron emission tomography (PET) studies.



Scheme 1. Synthesis of F- and CF₃-substituted 2,4-PDCA derivatives. Reagents and conditions: a) SOCl₂, MeOH, reflux, 59–93%; b) CO (1.5 atm), Cl₂Pd-*rac*-BINAP (1 mol%), Hünig's base, MeOH, 100 °C (sand bath temperature, sealed flask), 89–94%; c) LiOH, MeOH/H₂O, 0 °C to rt, 86–99%.

3. Conclusions

F- or CF₃-substituted derivatives of the broad-spectrum 2OG oxygenase inhibitor 2,4-PDCA were synthesized and their inhibitory activity determined for a set of human 2OG hydroxylases, which were already known to bind 2,4-PDCA [14, 24, 25]. Both the C3 and C5 F-substituted 2,4-PDCA derivatives were efficient AspH and KDM4E inhibitors, displaying a similar potency as 2,4-PDCA for AspH inhibition and an about fourfold reduced potency compared to 2,4-PDCA for KDM4E inhibition. Unlike 2,4-PDCA, the F- or CF₃-substituted 2,4-PDCA derivatives investigated did not inhibit FIH or RIOX2. The selectivity profile of the F- and CF₃-substituted 2,4-PDCA derivatives is similar to that of 2,4-PDCA, with the exceptions of 2,4-PDCA derivatives **8** and **14** for which a substantial increase in selectivity for AspH over KDM4E was observed, whilst in the case of **8** (but not **14**) maintaining potent AspH inhibition; an unprecedented observation with respect to 2OG oxygenase inhibition by 2,4-PDCA derivatives [15, 20]. Crystallographic analyses provide a rationale for the observed selectivity increase and thus will help to enable the design of more selective AspH inhibitors suitable for *in vivo* use.

4. Experimental

4.1. General information

Unless otherwise stated, all reagents were from commercial sources (Sigma-Aldrich, Inc.; Fluorochem Ltd) and used as received. Anhydrous solvents were from Sigma-Aldrich, Inc. and kept under an atmosphere of nitrogen. Solvents, liquids, and solutions were transferred using nitrogen-flushed stainless steel needles and syringes. Milli-Q® Ultrapure (MQ-grade) water was used for buffers; LCMS grade solvents (Merck) were used for solid phase extraction coupled to mass spectrometry (SPE-MS).

Purifications were performed using an automated Biotage Isolera One purification machine (wavelength monitored: 254 and 280 nm) equipped with pre-packed Biotage® SNAP KP-Sil or Biotage® SNAP Ultra flash chromatography cartridges. The cartridge size and solvent gradients (in column volumes, CV) used, are specified in the individual experimental procedures. HPLC grade solvents (ethyl acetate and cyclohexane; Sigma-Aldrich Inc.) were used for reaction work-ups, extractions, and purifications.

Thin layer chromatography (TLC) was carried out using Merck silica gel 60 F₂₅₄ TLC plates and visualized under UV light. Melting points (m. p.) were determined using a Stuart SMP-40 automated melting point

apparatus. Infrared (IR) spectroscopy was performed using a Bruker Tensor-27 Fourier transform infrared (FT-IR) spectrometer. High-resolution mass spectrometry (HRMS) was performed using electrospray ionization (ESI) mass spectrometry (MS) in the positive or negative ionization modes employing a Thermo Scientific Exactive mass spectrometer (ThermoFisher Scientific); data are presented as a mass-to-charge ratio (*m/z*).

Nuclear magnetic resonance (NMR) spectroscopy was performed using a Bruker AVANCE AVIIIHD 600 machine equipped with a 5 mm BB-F/1H Prodigy N₂ cryoprobe. Chemical shifts for protons are reported in parts per million (ppm) downfield from tetramethylsilane and are referenced to residual protium in the NMR solvent (CDCl₃: δ = 7.28 ppm; D₂O: δ = 4.79 ppm). For ¹³C NMR, chemical shifts are reported in the scale relative to the NMR solvent (*i.e.* CDCl₃: δ = 77.00 ppm). For ¹⁹F NMR, chemical shifts are reported in the scale relative to CFCl₃. NMR data are reported as follows: chemical shift, multiplicity (s: singlet, d: doublet, dd: doublet of doublets, t: triplet, q: quartet, m: multiplet), coupling constant (*J*, Hz; accurate to 0.1 Hz), and integration. ¹³C NMR chemical shift numbers in brackets indicate close signals that can be differentiated taking into account second decimal numbers.

4.2. General procedures

4.2.1. General procedure A

Thionyl chloride (1.5 equiv.) was added dropwise to a solution of 3- or 5-fluoro-2-chloroisonicotinic acid (1.0 equiv.) in anhydrous methanol (0.6 M) at ambient temperature under a nitrogen atmosphere. The reaction mixture was stirred under reflux for 2 h, then cooled to ambient temperature and concentrated. The residue was dissolved in ethyl acetate, washed twice with saturated aqueous NaHCO₃ solution, then once with brine. The organic solution was dried over anhydrous Na₂SO₄, filtered, evaporated, and purified by column chromatography to afford the corresponding methyl esters which were used in the next reaction following General Procedure B.

4.2.2. General procedure B

N,N-Diisopropylethylamine (Hünig's base; 1.5 equiv.) was added to a solution of a C3 or C5 fluoro/trifluoromethyl-substituted methyl 2-chloroisonicotinate (1.0 equiv.) and dichloro[2,2'-bis(diphenylphosphino)-1,1'-binaphthyl]palladium(II) [(*rac*-BINAP)PdCl₂] (0.01 equiv.) in anhydrous methanol (0.2 M) in a 250 mL J-Young Schlenk tube under an ambient temperature. Carbon monoxide gas (synthesis grade) was bubbled through the solution for 10 minutes. **Caution:** Carbon monoxide is a highly toxic and flammable gas; it should be handled in a well-

vented fume cupboard taking appropriate safety measures. The Schlenk tube was then sealed under CO-pressure (~1.5–2.0 atm) and placed in a sand bath; the tube was then heated with stirring behind a safety shield at 100 °C for 18–20 h. The reaction mixture was cooled to ambient temperature, then concentrated and purified by column chromatography to afford the corresponding C3 or C5 fluoro/trifluoromethyl-substituted dimethyl pyridine-2,4-dicarboxylates which were used in the next reaction following General Procedure C.

4.2.3. General procedure C

An aqueous solution of lithium hydroxide (0.4 M, 2.8 equiv.) was added to a solution of C3 or C5 fluoro/trifluoromethyl-substituted dimethyl pyridine-2,4-dicarboxylate (1.0 equiv.) in methanol (0.2 M, HPLC grade) under an ambient atmosphere at 0 °C. The reaction mixture was allowed to slowly warm to ambient temperature overnight (14–18 h). The methanol was then removed under reduced pressure. The aqueous reaction mixture was extracted three times with dichloromethane (the organic extracts were discarded) and the aqueous phase was acidified (pH ≈ 7.0 to 7.7) using Dowex® 50XW8 (H⁺-form, mesh 200–400). The mixture was filtered and lyophilized to afford the solid C3 or C5 fluoro/trifluoromethyl-substituted pyridine-2,4-dicarboxylate. The crude product was sufficiently pure as judged by ¹H and ¹³C NMR and used without further purification in the biological assays. pK_a-values for the 2,4-PDCA derivatives were not determined, thus, some might have actually been isolated as the corresponding mono- or dilithium salts.

4.3. Synthetic procedures and analytical data

4.3.1. Methyl 2-chloro-3-fluoroisonicotinate (15)

According to General Procedure A, methyl ester **15** (0.68 g, 59%) was obtained from commercially sourced 2-chloro-3-fluoroisonicotinic acid **3** (1.06 g, 6.0 mmol), following column chromatography (10 g Ultra cartridge; 35 mL/min; initially, 100% cyclohexane (2 column volumes, CV), followed by a linear gradient (15 CV): 0%→20% ethyl acetate in cyclohexane). White solid, m.p.: 43–45 °C; ¹H NMR (600 MHz, 300 K, CDCl₃): δ = 8.31 (d, *J* = 4.9 Hz, 1H), 7.71 (t, *J* = 4.8 Hz, 1H), 3.99 ppm (s, 3H); ¹⁹F NMR (565 MHz, 300 K, CDCl₃): δ = -116.2 ppm (d, *J* = 4.1 Hz, 1F); ¹³C NMR (150 MHz, 300 K, CDCl₃): δ = 162.4 (d, *J* = 3.3 Hz), 152.8 (d, *J* = 274.1 Hz), 144.5 (d, *J* = 7.7 Hz), 141.2 (d, *J* = 20.7 Hz), 127.1 (d, *J* = 9.6 Hz), 123.9, 53.2 ppm (d, *J* = 2.2 Hz); IR (film): ν̄ = 3109, 3022, 2966, 1732, 1458, 1429, 1397, 1272, 1257, 1204, 1136, 1086, 977 cm⁻¹; HRMS (ESI): *m/z* calculated for C₇H₆O₂NClF [M+H]⁺: 190.0066, found: 190.068.

4.3.2. Dimethyl 3-fluoropyridine-2,4-dicarboxylate (5)

According to General Procedure B, dimethyl ester **5** (0.72 g, 94%) was obtained from methyl 2-chloro-3-fluoroisonicotinate (**15**) (0.68 g, 3.6 mmol), following column chromatography (25 g KP-Sil cartridge; 50 mL/min; initially, 100% cyclohexane (3 CV), followed by a linear gradient (10 CV): 0%→50% ethyl acetate in cyclohexane). Pale yellow solid, m.p.: 57–59 °C; ¹H NMR (600 MHz, 300 K, CDCl₃): δ = 8.65 (d, *J* = 4.7 Hz, 1H), 7.96 (t, *J* = 4.8 Hz, 1H), 4.05 (s, 3H), 4.02 ppm (s, 3H); ¹⁹F NMR (565 MHz, 300 K, CDCl₃): δ = -118.3 ppm (d, *J* = 5.9 Hz, 1F); ¹³C NMR (150 MHz, 300 K, CDCl₃): δ = 162.9 (d, *J* = 6.0 Hz), 162.7 (d, *J* = 2.1 Hz), 157.0 (d, *J* = 283.0 Hz), 145.3 (d, *J* = 7.3 Hz), 138.9 (d, *J* = 11.0 Hz), 128.3, 127.9 (d, *J* = 10.1 Hz), 53.3, 53.2 ppm; IR (film): ν̄ = 3009, 2958, 1736, 1466, 1437, 1418, 1324, 1283, 1238, 1205, 1177, 1136, 1086, 993, 956 cm⁻¹; HRMS (ESI): *m/z* calculated for C₉H₉O₄NF [M+H]⁺: 214.0510, found: 214.0511.

4.3.3. 3-Fluoropyridine-2,4-dicarboxylic acid (7)

Dicarboxylic acid **7** (160 mg, 86%) was obtained from dimethyl 3-fluoropyridine-2,4-dicarboxylate **5** (213 mg, 1.0 mmol) according to General Procedure C. White solid, m.p.: >230 °C (decomposition); ¹H NMR (600 MHz, 300 K, D₂O): δ = 8.42 (d, *J* = 4.9 Hz, 1H), 7.67 ppm (t, *J*

= 5.0 Hz, 1H); ¹⁹F NMR (565 MHz, 300 K, D₂O): δ = -128.1 ppm (d, *J* = 4.1 Hz, 1F); ¹³C NMR (150 MHz, 300 K, D₂O): δ = 169.8, 169.2 (d, *J* = 3.5 Hz), 153.1 (d, *J* = 259.9 Hz), 143.8 (d, *J* = 5.7 Hz), 143.1 (d, *J* = 19.0 Hz), 137.1 (d, *J* = 16.2 Hz), 124.8 ppm (d, *J* = 5.4 Hz); IR (film): ν̄ = 3352, 1596, 1551, 1462, 1372, 1241, 1226, 1181, 1089 cm⁻¹; HRMS (ESI): *m/z* calculated for C₇H₃O₄NF [M-H]⁻: 184.0052, found: 184.0047.

4.3.4. Methyl 2-chloro-5-fluoroisonicotinate (16)

According to General Procedure A, methyl ester **16** (2.67 g, 93%) was obtained from commercially sourced 2-chloro-5-fluoroisonicotinic acid **4** (2.67 g, 15.2 mmol), following column chromatography (50 g KP-Sil cartridge; 50 mL/min; initially, 100% cyclohexane (2 CV), followed by a linear gradient (8 CV): 0%→20% ethyl acetate in cyclohexane). White solid, m.p.: 49–51 °C; ¹H NMR (600 MHz, 300 K, CDCl₃): δ = 8.41 (s, 1H), 7.81 (d, *J* = 5.0 Hz, 1H), 4.00 ppm (s, 3H); ¹⁹F NMR (565 MHz, 300 K, CDCl₃): δ = -128.4 ppm (d, *J* = 4.8 Hz, 1F); ¹³C NMR (150 MHz, 300 K, CDCl₃): δ = 162.1 (d, *J* = 3.4 Hz), 156.3 (d, *J* = 268.4 Hz), 146.7 (d, *J* = 4.1 Hz), 140.0 (d, *J* = 28.0 Hz), 128.2 (d, *J* = 10.5 Hz), 125.4, 53.3 ppm (d, *J* = 1.6 Hz); IR (film): ν̄ = 3098, 3031, 2961, 1721, 1462, 1438, 1357, 1269, 1246, 1212, 1132, 1083, 961 cm⁻¹; HRMS (ESI): *m/z* calculated for C₇H₆O₂NClF [M+H]⁺: 190.0066, found: 190.0068.

4.3.5. Dimethyl 5-fluoropyridine-2,4-dicarboxylate (6)

According to General Procedure B, dimethyl ester **6** (1.64 g, 89%) was obtained from methyl 2-chloro-5-fluoroisonicotinate (**16**) (1.9 g, 10.0 mmol), following column chromatography (50 g KP-Sil cartridge; 50 mL/min; initially, 100% cyclohexane (2 CV), followed by a linear gradient (12 CV): 0%→100% ethyl acetate in cyclohexane). White solid, m.p.: 87–89 °C; ¹H NMR (600 MHz, 300 K, CDCl₃): δ = 8.72 (d, *J* = 1.7 Hz, 1H), 8.63 (d, *J* = 5.8 Hz, 1H), 4.04 (s, 3H), 4.02 ppm (s, 3H); ¹⁹F NMR (565 MHz, 300 K, CDCl₃): δ = -118.4 ppm (d, *J* = 5.6 Hz, 1F); ¹³C NMR (150 MHz, 300 K, CDCl₃): δ = 164.0, 162.4 (d, *J* = 3.1 Hz), 158.8 (d, *J* = 276.2 Hz), 144.5 (d, *J* = 5.4 Hz), 140.8 (d, *J* = 26.5 Hz), 127.0, 126.1 (d, *J* = 8.8 Hz), 53.2 (d, *J* = 2.2 Hz), 53.1(9) ppm (d, *J* = 2.2 Hz); IR (film): ν̄ = 3085, 3040, 3018, 2961, 1733, 1720, 1607, 1561, 1467, 1447, 1433, 1402, 1310, 1259, 1242, 1213, 1139, 1082, 991, 956 cm⁻¹; HRMS (ESI): *m/z* calculated for C₉H₉O₄NF [M+H]⁺: 214.0510, found: 214.0511.

4.3.6. 5-Fluoropyridine-2,4-dicarboxylic acid (8)

Dicarboxylic acid **8** (184 mg, 99%) was obtained from dimethyl 5-fluoropyridine-2,4-dicarboxylate **6** (213 mg, 1.0 mmol), along with some minor impurities which were not separated, according to General Procedure C. White solid, m.p.: >270 °C (decomposition); ¹H NMR (600 MHz, 300 K, D₂O): δ = 8.51 (d, *J* = 1.2 Hz, 1H), 8.06 ppm (d, *J* = 5.8 Hz, 1H); ¹⁹F NMR (565 MHz, 300 K, D₂O): δ = -128.5 ppm (d, *J* = 5.6 Hz, 1F); ¹³C NMR (150 MHz, 300 K, D₂O): δ = 171.7, 170.3, 156.7 (d, *J* = 259.8 Hz), 149.9 (d, *J* = 5.0 Hz), 138.1 (d, *J* = 27.2 Hz), 134.4 (d, *J* = 14.2 Hz), 123.6 ppm; IR (film): ν̄ = 3245, 1603, 1436, 1380, 1296, 1221, 1096 cm⁻¹; HRMS (ESI): *m/z* calculated for C₇H₃O₄NF [M-H]⁻: 184.0052, found: 184.0047.

4.3.7. Dimethyl 3-trifluoromethylpyridine-2,4-dicarboxylate (11)

According to General Procedure B, dimethyl ester **11** (0.99 g, 89%) was obtained from commercially sourced methyl 2-chloro-3-trifluoromethylisonicotinate (**9**) (1.0 g, 4.2 mmol), following column chromatography (25 g KP-Sil cartridge; 50 mL/min; initially, 100% cyclohexane (3 CV), followed by a linear gradient (20 CV): 0%→40% ethyl acetate in cyclohexane). Pale yellow solid, m.p.: 48–50 °C; ¹H NMR (600 MHz, 300 K, CDCl₃): δ = 8.90 (d, *J* = 4.9 Hz, 1H), 7.65 (d, *J* = 4.9 Hz, 1H), 4.03 (s, 3H), 4.00 ppm (s, 3H); ¹⁹F NMR (565 MHz, 300 K, CDCl₃): δ = -56.8 ppm (s, 3F); ¹³C NMR (150 MHz, 300 K, CDCl₃): δ = 165.5, 165.4, 152.5, 150.5 (q, *J* = 2.6 Hz), 140.9 (q, *J* = 2.4 Hz), 123.8, 122.1 (q, *J* = 274.7 Hz), 121.6 (q, *J* = 34.8 Hz), 53.6 (q, *J* = 8.4 Hz), 53.5 ppm (q, *J* = 8.3

Hz); IR (film): $\tilde{\nu}$ = 3015, 2960, 1743, 1588, 1560, 1437, 1415, 1320, 1297, 1272, 1214, 1187, 1148, 1109, 1034, 988, 955 cm^{-1} ; HRMS (ESI): m/z calculated for $\text{C}_{10}\text{H}_9\text{O}_4\text{NF}_3$ $[\text{M}+\text{H}]^+$: 264.0478, found: 264.0478.

4.3.8. 3-Trifluoromethylpyridine-2,4-dicarboxylic acid (**13**)

Dicarboxylic acid **13** (210 mg, 89%) was obtained from dimethyl 3-trifluoromethylpyridine-2,4-dicarboxylate **11** (263 mg, 1.0 mmol) according to General Procedure C. White solid, m.p.: >220 °C (decomposition); ^1H NMR (600 MHz, 300 K, D_2O): δ = 8.68 (d, J = 5.1 Hz, 1H), 7.46 ppm (d, J = 5.1 Hz, 1H); ^{19}F NMR (565 MHz, 300 K, D_2O): δ = -57.4 ppm (s, 3F); ^{13}C NMR (150 MHz, 300 K, D_2O): δ = 173.5, 173.2, 155.5 (q, J = 2.9 Hz), 151.8, 148.3 (q, J = 2.7 Hz), 123.0 (q, J = 273.9 Hz), 120.6, 115.6 ppm (q, J = 32.8 Hz); IR (film): $\tilde{\nu}$ = 3358, 1591, 1555, 1462, 1375, 1289, 1239, 1136, 1117, 1039 cm^{-1} ; HRMS (ESI): m/z calculated for $\text{C}_8\text{H}_3\text{O}_4\text{NF}_3$ $[\text{M}-\text{H}]^-$: 234.0020, found: 234.0020.

4.3.9. Dimethyl 5-trifluoromethylpyridine-2,4-dicarboxylate (**12**)

According to General Procedure B, dimethyl ester **12** (1.03 g, 93%) was obtained from commercially sourced methyl 2-chloro-5-trifluoromethylisonicotinate (**10**) (1.0 g, 4.2 mmol), following column chromatography (25 g KP-Sil cartridge; 50 mL/min; initially, 100% cyclohexane (3 CV), followed by a linear gradient (15 CV): 0%–30% ethyl acetate in cyclohexane). Pale yellow solid, m.p.: 58–60 °C; ^1H NMR (600 MHz, 300 K, CDCl_3): δ = 9.13 (s, 1H), 8.45 (s, 1H), 4.08 (s, 3H), 4.02 ppm (s, 3H); ^{19}F NMR (565 MHz, 300 K, CDCl_3): δ = -59.8 ppm (s, 3F); ^{13}C NMR (150 MHz, 300 K, CDCl_3): δ = 164.4, 163.8, 151.6, 148.1 (q, J = 5.6 Hz), 140.0 (q, J = 2.1 Hz), 126.1 (q, J = 33.3 Hz), 124.5, 122.2 (q, J = 274.4 Hz), 53.6, 53.5 ppm; IR (film): $\tilde{\nu}$ = 3117, 3022, 2964, 1749, 1727, 1598, 1567, 1489, 1428, 1373, 1331, 1251, 1148, 1129, 1111, 1037, 982, 956 cm^{-1} ; HRMS (ESI): m/z calculated for $\text{C}_{10}\text{H}_9\text{O}_4\text{NF}_3$ $[\text{M}+\text{H}]^+$: 264.0478, found: 264.0479.

4.3.10. 5-Trifluoromethylpyridine-2,4-dicarboxylic acid (**14**)

Dicarboxylic acid **14** (226 mg, 96%) was obtained from dimethyl 5-trifluoromethylpyridine-2,4-dicarboxylate **12** (263 mg, 1.0 mmol) according to General Procedure C. White solid, m.p.: >260 °C (decomposition); ^1H NMR (600 MHz, 300 K, D_2O): δ = 8.91 (s, 1H), 7.90 ppm (s, 1H); ^{19}F NMR (565 MHz, 300 K, D_2O): δ = -60.1 ppm (s, 3F); ^{13}C NMR (150 MHz, 300 K, D_2O): δ = 173.2, 171.4, 157.3, 147.7 (q, J = 2.4 Hz), 146.6 (q, J = 5.0 Hz), 123.2 (q, J = 273.0 Hz), 121.6 (q, J = 32.3 Hz), 120.3 ppm; IR (film): $\tilde{\nu}$ = 3427, 1601, 1557, 1441, 1390, 1361, 1321, 1279, 1199, 1158, 1138, 1045 cm^{-1} .

4.4. 2OG oxygenase inhibition assays

SPE-MS inhibition assays using human *N*-terminally His₆-tagged AspH_{315–758} [14, 28], *N*-terminally His₆-tagged FIH [29], and KDM4E [15, 31] were performed in independent duplicates as described in the cited literature; The standard deviation (SD) of two independent IC₅₀ determinations ($n = 2$), each composed of technical duplicates, was calculated using GraphPad Prism 5. 2OG oxygenases were produced and purified as described in the cited literature, the peptide substrate for AspH was synthesized according to the cited literature while the peptide substrates for FIH and KDM4E were obtained from GL Biochem (Shanghai) Ltd (Shanghai, China). All peptide were prepared with C-terminal amides.

SPE-MS inhibition assays using recombinant human *N*-terminally His₆-tagged RIOX2_{26–465} (human wild-type RIOX2 (amino acid sequence: 26–465) was produced in *E. coli* BL21 (DE3) cells using a pET-28a(+) vector and purified as reported [18, 26]) were performed as described below using the RPL27A_{31–49} substrate peptide (amino acids 31–49 of human RPL27A: GRGNAGGLHHHRINFDFKYHP, H39 is the hydroxylation site of RIOX2 [18]; synthesized and purified by GL Biochem (Shanghai) Ltd from Shanghai, China). Details of the RIOX2 assay will be reported elsewhere [30].

Solutions of the 2OG derivatives (100% DMSO) were dry dispensed

across 384-well polypropylene assay plates (Greiner) in a threefold and 11-point dilution series (100 μM top concentration) using an ECHO 550 acoustic dispenser (Labcyte). DMSO and 2,4-PDCA were used as negative and positive inhibition controls, respectively. The final DMSO concentration was kept constant at 0.5%_{v/v} throughout all experiments (using the DMSO backfill option of the acoustic dispenser). Each reaction was performed in technical duplicates in adjacent wells of the assay plates; additionally, assays were performed in two independent duplicates on different days using different DMSO inhibitor solutions. Cosubstrate/cofactor stock solutions (L-ascorbic acid, LAA: 50 mM in MQ-grade water; 2-oxoglutarate, 2OG: 10 mM in MQ-grade water; ammonium iron(II) sulfate hexahydrate, FAS, $(\text{NH}_4)_2\text{Fe}(\text{SO}_4)_2 \cdot 6\text{H}_2\text{O}$: 400 mM in 20 mM HCl diluted to 1 mM in MQ-grade water) were freshly prepared each day from commercially sourced solids (Sigma Aldrich).

The Enzyme Mixture (25 μL /well), containing His₆-RIOX2_{26–465} (0.3 μM) in reaction buffer (50 mM HEPES, 50 mM NaCl, pH 7.5), was dispensed across the inhibitor-containing 384-well assay plates with a multidrop dispenser (ThermoFischer Scientific) at 20 °C under an ambient atmosphere. The plates were subsequently centrifuged (1000 rpm, 20 s) and incubated for 15 minutes at 20 °C. The Substrate Mixture (25 μL /well), containing RPL27A_{31–49} substrate peptide (10 μM), LAA (200 μM), 2OG (20 μM), and FAS (20 μM) in reaction buffer, was added using the multidrop dispenser. The plates were centrifuged (1000 rpm, 20 s) and, after incubating for 30 minutes, the enzyme reaction was stopped by the addition of 10%_{v/v} aqueous formic acid (5 μL /well). The plates were then centrifuged (1000 rpm, 30 s) and analysed by MS.

MS-analyses were performed using a RapidFire RF 365 high-throughput sampling robot (Agilent) attached to an iFunnel Agilent 6550 accurate mass quadrupole time-of-flight (Q-TOF) mass spectrometer operated in the positive ionization mode. Assay samples were aspirated under vacuum for 0.6 s and loaded onto a C4 solid phase extraction (SPE) cartridge. After loading, the C4 SPE cartridge was washed with 0.1%_{v/v} aqueous formic acid to remove non-volatile buffer salts (5.5 s, 1.5 mL/min). The peptide was eluted from the SPE cartridge with 0.1%_{v/v} formic acid in 80/20_{v/v} acetonitrile/water into the mass spectrometer (5.5 s, 1.4 mL/min) and the SPE cartridge re-equilibrated with 0.1%_{v/v} aqueous formic acid (0.5 s, 1.25 mL/min). The mass spectrometer parameters were: capillary voltage (4000 V), nozzle voltage (1000 V), fragmentor voltage (365 V), gas temperature (280 °C), gas flow (13 L/min), sheath gas temperature (350 °C), sheath gas flow (12 L/min), nebulizer pressure (40 psig). The m/z +4 charge states of the RPL27A_{31–49} substrate peptide and the hydroxylated product peptide were used to extract ion chromatogram data, peak areas were integrated using RapidFire Integrator software (Agilent). Data were exported into Microsoft Excel and used to calculate the % conversion of the hydroxylation reaction using the equation: % conversion = 100 x (integral hydroxylated product peptide) / (integral RPL27A_{31–49} substrate peptide + integral hydroxylated product peptide). Normalized dose-response curves (2,4-PDCA and DMSO controls) were obtained from the raw data by non-linear regression (GraphPad Prism 5) and used to determine IC₅₀-values. The SD of two independent IC₅₀ determinations ($n = 2$) was calculated using GraphPad Prism 5.

4.5. Crystallography and structure solutions

High-throughput crystallization experiments were performed in 96-well, 3-subwell, low profile Intelliplates (Art Robbins Instruments) using a Phoenix RE liquid dispensing robot (Art Robbins Instruments) and the PACT Premier crystallization screen (Molecular Dimensions). *N*-Terminally His₆-tagged AspH_{315–758} (0.33 mM in 50 mM HEPES buffer, pH 7.5) was mixed with 1 mM MnCl_2 , 2 mM fluorinated 2,4-PDCA derivative, and the hFX-EGFD1_{86–124}-4Ser peptide [6] (0.73 mM; Supporting Figure S4) as AspH substrate. Crystals were grown using the vapor diffusion method at 4 °C in 200 nL or 300 nL sitting drops with 2:1, 1:1 or 1:2 sample:well solution ratios; precipitants are listed in the Supporting Table S1. Crystals were cryo-protected using mother liquor

supplemented with 20%_{v/v} glycerol before cryo-cooling in liquid N₂. Data were collected at 100 K using synchrotron radiation at Diamond Light Source (DLS) beamlines I03 and I24. Data were indexed, integrated, and scaled using the Xia2 [53] strategy of the beamline auto-processing pipeline (Supporting Table S1).

The AspH crystal structures were determined by molecular replacement (MR) using the AutoMR (PHASER [54]) subroutine in PHENIX [55]. The search model used for MR was based on PDB ID 5JTC [14]. The structural model was improved by iterative cycles of manual re-building in COOT [56] and crystallographic refinement in phenix.refine [57] (refinement details are summarized in Supporting Table S1).

Crystal structure data for *N*-terminal His₆-tagged AspH_{315–758} complexed to Mn, the fluorinated 2,4-PDCA derivatives (3-fluoropyridine-2,4-dicarboxylic acid, **7**; 5-fluoropyridine-2,4-dicarboxylic acid, **8**), and substrate peptide (hFX-EGFD1_{86–124}-4Ser) are deposited in the protein data bank with PDB accession codes: 7MBI (AspH:7) and 7MBJ (AspH:8). PyMOL [58] was used for the generation of graphical representations; polder omit maps were calculated using Polder Maps [59] in PHENIX [55].

Declaration of Competing Interest

The authors declare that they have no known competing financial interests or personal relationships that could have appeared to influence the work reported in this paper.

Acknowledgments

This research was funded in part by the Wellcome Trust (106244/Z/14/Z). For the purpose of open access, the author has applied a CC BY public copyright license to any Author Accepted Manuscript version arising from this submission. We thank Cancer Research UK (C8717/A18245) and the Biotechnology and Biological Sciences Research Council (BB/J003018/1 and BB/R000344/1) for funding. L.B. thanks the Deutsche Forschungsgemeinschaft for a fellowship (BR 5486/2-1). Y.N. thanks the JSPS for an Overseas Research Fellowship (2020060219) and the Daiichi Sankyo Foundation of Life Science. We thank the Diamond Light Source and staff for allocation of beam time and support.

Supplementary materials

Supplementary material associated with this article can be found, in the online version, at doi:10.1016/j.jfluchem.2021.109804.

References

- R.P. Hausinger, C.J. Schofield (Eds.), *2-Oxoglutarate-Dependent Oxygenases*, The Royal Society of Chemistry, Cambridge, 2015.
- W.G. Kaelin Jr., P.J. Ratcliffe, Oxygen sensing by metazoans: The central role of the HIF hydroxylase pathway, *Mol. Cell* 30 (4) (2008) 393–402.
- S. Dhillion, Roxadustat: First global approval, *Drugs* 79 (5) (2019) 563–572.
- N.R. Rose, M.A. McDonough, O.N.F. King, A. Kawamura, C.J. Schofield, Inhibition of 2-oxoglutarate dependent oxygenases, *Chem. Soc. Rev.* 40 (8) (2011) 4364–4397.
- J. Stenflo, E. Holme, S. Lindstedt, N. Chandramouli, L.H. Tsai Huang, J.P. Tam, R. B. Merrifield, Hydroxylation of aspartic acid in domains homologous to the epidermal growth factor precursor is catalyzed by a 2-oxoglutarate-dependent dioxygenase, *Proc. Natl. Acad. Sci. USA* 86 (2) (1989) 444–447.
- I. Pfeffer, L. Brewitz, T. Krojer, S.A. Jensen, G.T. Kochan, N.J. Kershaw, K. S. Hewitson, L.A. McNeill, H. Kramer, M. Münzel, R.J. Hopkinson, U. Oppermann, P.A. Handford, M.A. McDonough, C.J. Schofield, Aspartate/asparagine- β -hydroxylase crystal structures reveal an unexpected epidermal growth factor-like domain substrate disulfide pattern, *Nat. Commun.* 10 (1) (2019) 4910.
- L. Brewitz, A. Tumber, C.J. Schofield, Kinetic parameters of human aspartate/asparagine- β -hydroxylase suggest that it has a possible function in oxygen sensing, *J. Biol. Chem.* 295 (23) (2020) 7826–7838.
- M. Kanwal, M. Smahel, M. Olsen, J. Smahelova, R. Tachezy, Aspartate β -hydroxylase as a target for cancer therapy, *J. Exp. Clin. Cancer Res.* 39 (1) (2020) 163.
- Y. Zheng, X. Wang, J. Hu, B. Bai, H. Zhu, Diverse molecular functions of aspartate β -hydroxylase in cancer, *Oncol. Rep.* 44 (6) (2020) 2364–2372.
- H.Ü. Kaniskan, M.L. Martini, J. Jin, Inhibitors of protein methyltransferases and demethylases, *Chem. Rev.* 118 (3) (2018) 989–1068.
- H. Lin, Q. Li, Q. Li, J. Zhu, K. Gu, X. Jiang, Q. Hu, F. Feng, W. Qu, Y. Chen, H. Sun, Small molecule KDM4s inhibitors as anti-cancer agents, *J. Enzyme Inhib. Med. Chem.* 33 (1) (2018) 777–793.
- R.P. Nowak, A. Tumber, C. Johansson, K.H. Che, P. Brennan, D. Owen, U. Oppermann, Advances and challenges in understanding histone demethylase biology, *Curr. Opin. Chem. Biol.* 33 (2016) 151–159.
- K. Al-Qahtani, B. Jabeen, R. Sekirnik, N. Riaz, T.D.W. Claridge, C.J. Schofield, J.S. O. McCullagh, The broad spectrum 2-oxoglutarate oxygenase inhibitor N-oxalylglycine is present in rhubarb and spinach leaves, *Phytochemistry* 117 (2015) 456–461.
- L. Brewitz, A. Tumber, I. Pfeffer, M.A. McDonough, C.J. Schofield, Aspartate/asparagine- β -hydroxylase: a high-throughput mass spectrometric assay for discovery of small molecule inhibitors, *Sci. Rep.* 10 (1) (2020) 8650.
- L. Brewitz, A. Tumber, A. Thalhammer, E. Salah, K.E. Christensen, C.J. Schofield, Synthesis of novel pyridine-carboxylates as small-molecule inhibitors of human aspartate/asparagine- β -hydroxylase, *ChemMedChem* 15 (2020) 1139–1149.
- H. Choi, A.P. Hardy, T.M. Leissing, R. Chowdhury, Y. Nakashima, W. Ge, M. Markoulides, J.S. Scotti, P.A. Gerken, H. Thorbjørnsrud, D. Kang, S. Hong, J. Lee, M.A. McDonough, H. Park, C.J. Schofield, A human protein hydroxylase that accepts D-residues, *Commun. Chem.* 3 (1) (2020) 52.
- K.S. Hewitson, L.A. McNeill, M.V. Riordan, Y.-M. Tian, A.N. Bullock, R.W. Welford, J.M. Elkins, N.J. Oldham, S. Bhattacharya, J.M. Gleadle, P.J. Ratcliffe, C.W. Pugh, C.J. Schofield, Hypoxia-inducible Factor (HIF) asparagine hydroxylase is identical to factor inhibiting HIF (FIH) and is related to the cupin structural family, *J. Biol. Chem.* 277 (29) (2002) 26351–26355.
- W. Ge, A. Wolf, T. Feng, C.-h. Ho, R. Sekirnik, A. Zayer, N. Granatino, M. E. Cockman, C. Loenarz, N.D. Loik, A.P. Hardy, T.D.W. Claridge, R.B. Hamed, R. Chowdhury, L. Gong, C.V. Robinson, D.C. Trudjian, M. Jiang, M.M. Mackeen, J. S. McCullagh, Y. Gordiyenko, A. Thalhammer, A. Yamamoto, M. Yang, P. Liu-Yi, Z. Zhang, M. Schmidt-Zachmann, B.M. Kessler, P.J. Ratcliffe, G.M. Preston, M. L. Coleman, C.J. Schofield, Oxygenase-catalyzed ribosome hydroxylation occurs in prokaryotes and humans, *Nat. Chem. Biol.* 8 (12) (2012) 960–962.
- M.A. McDonough, L.A. McNeill, M. Tilliet, C.A. Papamicaël, Q.-Y. Chen, B. Banerji, K.S. Hewitson, C.J. Schofield, Selective inhibition of factor inhibiting hypoxia-inducible factor, *J. Am. Chem. Soc.* 127 (21) (2005) 7680–7681.
- A. Thalhammer, J. Mecinović, C. Loenarz, A. Tumber, N.R. Rose, T.D. Heightman, C.J. Schofield, Inhibition of the histone demethylase JMJD2E by 3-substituted pyridine 2,4-dicarboxylates, *Org. Biomol. Chem.* 9 (1) (2011) 127–135.
- E.P. Gillis, K.J. Eastman, M.D. Hill, D.J. Donnelly, N.A. Meanwell, Applications of fluorine in medicinal chemistry, *J. Med. Chem.* 58 (21) (2015) 8315–8359.
- H.-J. Böhm, D. Banner, S. Bendels, M. Kansy, B. Kuhn, K. Müller, U. Obst-Sander, M. Stahl, Fluorine in medicinal chemistry, *ChemBioChem* 5 (5) (2004) 637–643.
- J. Albaneze-Walker, C. Bazaral, T. Leavey, P.G. Dormer, J.A. Murry, Improved carbonylation of heterocyclic chlorides and electronically challenging aryl bromides, *Org. Lett.* 6 (13) (2004) 2097–2100.
- A. Conejo-Garcia, M.A. McDonough, C. Loenarz, L.A. McNeill, K.S. Hewitson, W. Ge, B.M. Liénard, C.J. Schofield, L.J. Clifton, Structural basis for binding of cyclic 2-oxoglutarate analogues to factor-inhibiting hypoxia-inducible factor, *Bioorg. Med. Chem. Lett.* 20 (20) (2010) 6125–6128.
- L. Hillringhaus, W.W. Yue, N.R. Rose, S.S. Ng, C. Gileadi, C. Loenarz, S.H. Bello, J. E. Bray, C.J. Schofield, U. Oppermann, Structural and evolutionary basis for the dual substrate selectivity of human KDM4 histone demethylase family, *J. Biol. Chem.* 286 (48) (2011) 41616–41625.
- R. Chowdhury, R. Sekirnik, N.C. Brissett, T. Krojer, C.-h. Ho, S.S. Ng, L.J. Clifton, W. Ge, N.J. Kershaw, G.C. Fox, J.R.C. Muniz, M. Vollmar, C. Phillips, E.S. Pilka, K. L. Kavanagh, F. von Delft, U. Oppermann, M.A. McDonough, A.J. Doherty, C. J. Schofield, Ribosomal oxygenases are structurally conserved from prokaryotes to humans, *Nature* 510 (7505) (2014) 422–426.
- K.E. Bräuer, K. Brockers, J. Moneer, A. Feuchtinger, E. Wollscheid-Lengeling, A. Lengeling, A. Wolf, Phylogenetic and genomic analyses of the ribosomal oxygenases RioX1 (No66) and RioX2 (Mina53) provide new insights into their evolution, *BMC Evol. Biol.* 18 (1) (2018) 96.
- L. Brewitz, A. Tumber, X. Zhang, C.J. Schofield, Small-molecule active pharmaceutical ingredients of approved cancer therapeutics inhibit human aspartate/asparagine- β -hydroxylase, *Bioorg. Med. Chem.* 28 (20) (2020), 115675.
- J.P. Holt-Martyn, R. Chowdhury, A. Tumber, T.-L. Yeh, M.I. Abboud, K. Lippl, C. T. Lohanz, G.W. Langley, W. Figg Jr., M.A. McDonough, C.W. Pugh, P.J. Ratcliffe, C.J. Schofield, Structure-activity relationship and crystallographic studies on 4-hydroxypyrimidine HIF prolyl hydroxylase domain inhibitors, *ChemMedChem* 15 (2020) 270–273.
- R.P. Nowak, A. Tumber, M.S.Z. Ansari, N. Mautone, A. Kawamura, C. Johansson, N. Giacché, D. Passeri, R. Pellicciari, D. Del Bufalo, M.L. Coleman, D. Trisciuglio, A. Mai, U. Oppermann, C.J. Schofield, D. Rotili, First-in-class inhibitors of the Ribosomal Oxygenase MINA53, manuscript under revision.
- S.E. Hutchinson, M.V. Leveridge, M.L. Heathcote, P. Francis, L. Williams, M. Gee, J. Munoz-Muriedas, B. Leavens, A. Shillings, E. Jones, P. Homes, S. Baddeley, C.-w. Chung, A. Bridges, A. Argyrou, Enabling lead discovery for histone lysine demethylases by high-throughput RapidFire mass spectrometry, *J. Biomol. Screen.* 17 (1) (2012) 39–48.
- J.-H. Zhang, T.D.Y. Chung, K.R. Oldenburg, A simple statistical parameter for use in evaluation and validation of high throughput screening assays, *J. Biomol. Screen.* 4 (2) (1999) 67–73.
- A.V. Hill, The possible effects of the aggregation of the molecules of haemoglobin on its dissociation curves, *J. Physiol.* 40 (1910) iv–vii.

- [34] Q. Zhang, C. Thakur, J. Shi, J. Sun, Y. Fu, P. Stemmer, F. Chen, New discoveries of mdg in the epigenetic regulation of cancers, *Semin. Cancer Biol.* 57 (2019) 27–35.
- [35] J.E. True, T.D. Thomas, R.W. Winter, G.L. Gard, Electronegativities from core-ionization energies: Electronegativities of SF₅ and CF₃, *Inorg. Chem.* 42 (14) (2003) 4437–4441.
- [36] Y. Carcenac, P. Diter, C. Wakselman, M. Tordeux, Experimental determination of the conformational free energies (A values) of fluorinated substituents in cyclohexane by dynamic ¹⁹F NMR spectroscopy. Part 1. Description of the method for the trifluoromethyl group, *New J. Chem.* 30 (3) (2006) 442–446.
- [37] G. Bott, L.D. Field, S. Sternhell, Steric effects. A study of a rationally designed system, *J. Am. Chem. Soc.* 102 (17) (1980) 5618–5626.
- [38] P. Fernlund, J. Stenflo, β-hydroxyaspartic acid in vitamin K-dependent proteins, *J. Biol. Chem.* 258 (20) (1983) 12509–12512.
- [39] B.A. McMullen, K. Fujikawa, W. Kisiel, T. Sasagawa, W.N. Howald, E.Y. Kwa, B. Weinstein, Complete amino acid sequence of the light chain of human blood coagulation factor X: evidence for identification of residue 63 as β-hydroxyaspartic acid, *Biochemistry* 22 (12) (1983) 2875–2884.
- [40] L. Brewitz, Y. Nakashima, C.J. Schofield, Synthesis of 2-oxoglutarate derivatives and their evaluation as cosubstrates and inhibitors of human aspartate/asparagine-β-hydroxylase, *Chem. Sci.* 12 (2021) 1327–1342.
- [41] N. Ince, S.M. de la Monte, J.R. Wands, Overexpression of human aspartyl (asparaginy) β-hydroxylase is associated with malignant transformation, *Cancer Res.* 60 (5) (2000) 1261–1266.
- [42] Q. Zou, Y. Hou, H. Wang, K. Wang, X. Xing, Y. Xia, X. Wan, J. Li, B. Jiao, J. Liu, A. Huang, D. Wu, H. Xiang, T.M. Pawlik, H. Wang, W.Y. Lau, Y. Wang, F. Shen, Hydroxylase activity of ASPH promotes hepatocellular carcinoma metastasis through epithelial-to-mesenchymal transition pathway, *EBioMedicine* 31 (2018) 287–298.
- [43] M.M. Mackeen, H.B. Kramer, K.-H. Chang, M.L. Coleman, R.J. Hopkinson, C. J. Schofield, B.M. Kessler, Small-molecule-based inhibition of histone demethylation in cells assessed by quantitative mass spectrometry, *J. Proteome Res.* 9 (8) (2010) 4082–4092.
- [44] H. Qi, Z. Jing, W. Xiaolin, X. Changwu, H. Xiaorong, Y. Jian, C. Jing, J. Hong, Histone demethylase JMJD2A inhibition attenuates neointimal hyperplasia in the carotid arteries of balloon-injured diabetic rats via transcriptional silencing: Inflammatory gene expression in vascular smooth muscle cells, *Cell. Physiol. Biochem.* 37 (2) (2015) 719–734.
- [45] L. Hu, Z. Li, J. Cheng, Q. Rao, W. Gong, M. Liu, Y.G. Shi, J. Zhu, P. Wang, Y. Xu, Crystal structure of TET2-DNA complex: Insight into TET-mediated 5mC oxidation, *Cell* 155 (7) (2013) 1545–1555.
- [46] C. Dalvit, Ligand- and substrate-based ¹⁹F NMR screening: Principles and applications to drug discovery, *Prog. Nucl. Magn. Reson. Spectrosc.* 51 (4) (2007) 243–271.
- [47] C. Dalvit, A. Vulpetti, Ligand-based fluorine NMR screening: Principles and applications in drug discovery projects, *J. Med. Chem.* 62 (5) (2019) 2218–2244.
- [48] M.G. Campbell, T. Ritter, Late-stage fluorination: From fundamentals to application, *Org. Process Res. Dev.* 18 (4) (2014) 474–480.
- [49] S. Preshlock, M. Tredwell, V. Gouverneur, ¹⁸F-Labeling of arenes and heteroarenes for applications in positron emission tomography, *Chem. Rev.* 116 (2) (2016) 719–766.
- [50] F. Dollé, Fluorine-18-labelled fluoropyridines: Advances in radiopharmaceutical design, *Curr. Pharm. Des.* 11 (25) (2005) 3221–3235.
- [51] P. Brugarolas, J.E. Sánchez-Rodríguez, H.-M. Tsai, F. Basuli, S.-H. Cheng, X. Zhang, A.V. Capriariello, J.J. Lacroix, R. Freifelder, D. Murali, O. DeJesus, R.H. Miller, R. E. Swenson, C.-T. Chen, P. Herscovitch, D.S. Reich, F. Bezanilla, B. Popko, Development of a PET radioligand for potassium channels to image CNS demyelination, *Sci. Rep.* 8 (1) (2018) 607.
- [52] M. Pauton, C. Aubert, G. Bluet, F. Gruss-Leleu, S. Roy, C. Perrio, Development, optimization, and scope of the radiosynthesis of 3/5-¹⁸F]fluoropyridines from readily prepared aryl(pyridinyl) iodonium salts: The importance of TEMPO and K₂CO₃, *Org. Process Res. Dev.* 23 (5) (2019) 900–911.
- [53] G. Winter, xia2: An expert system for macromolecular crystallography data reduction, *J. Appl. Cryst.* 43 (1) (2010) 186–190.
- [54] A.J. McCoy, R.W. Grosse-Kunstleve, P.D. Adams, M.D. Winn, L.C. Storoni, R. J. Read, Phaser crystallographic software, *J. Appl. Cryst.* 40 (4) (2007) 658–674.
- [55] P.D. Adams, P.V. Afonine, G. Bunkóczi, V.B. Chen, I.W. Davis, N. Echols, J. J. Headd, L.-W. Hung, G.J. Kapral, R.W. Grosse-Kunstleve, A.J. McCoy, N. W. Moriarty, R. Oeffner, R.J. Read, D.C. Richardson, J.S. Richardson, T. C. Terwilliger, P.H. Zwart, PHENIX: A comprehensive Python-based system for macromolecular structure solution, *Acta Cryst. D* 66 (2) (2010) 213–221.
- [56] P. Emsley, B. Lohkamp, W.G. Scott, K. Cowtan, Features and development of Coot, *Acta Cryst. D* 66 (4) (2010) 486–501.
- [57] P.V. Afonine, R.W. Grosse-Kunstleve, N. Echols, J.J. Headd, N.W. Moriarty, M. Mustyakimov, T.C. Terwilliger, A. Urzhumtsev, P.H. Zwart, P.D. Adams, Towards automated crystallographic structure refinement with phenix.refine, *Acta Cryst. D* 68 (4) (2012) 352–367.
- [58] W.L. DeLano, The PyMOL Molecular Graphics System, De Lano Scientific, San Carlos, 2002.
- [59] D. Liebschner, P.V. Afonine, N.W. Moriarty, B.K. Poon, O.V. Sobolev, T. C. Terwilliger, P.D. Adams, Polder maps: improving OMIT maps by excluding bulk solvent, *Acta Cryst. D* 73 (2) (2017) 148–157.